Synergistically-enhanced ion track formation in pre-damaged strontium titanate by energetic heavy ions

Haizhou Xue [a], Eva Zarkadoula [b], Ritesh Sachan [b], Yanwen Zhang [b], Christina Trautmann [c, d], and William J. Weber [a,b*]

[a] *Department of Materials Science & Engineering, University of Tennessee, Knoxville, Tennessee 37996, USA.*

[b] *Materials Science & Technology Division, Oak Ridge National Laboratory, Oak Ridge, Tennessee 37831, USA.*

[c] *GSI Helmholtzzentrum für Schwerionenforschung GmbH, Planckstrasse 1, Darmstadt 64291, Germany.*

[d] *Materialwissenschaft, Technische Universität Darmstadt, Darmstadt 64287, Germany.*

** To whom correspondence should be addressed:* wjweber@utk.edu

Abstract

Latent ion tracks created by energetic heavy ions (12 MeV Ti to 946 MeV Au) in single crystal $SrTiO_3$ are investigated using Rutherford backscattering spectrometry and scanning transmission electron microscopy. The results demonstrate that pre-existing irradiation damage, introduced via elastic collision processes, interacts

synergistically with the electronic energy deposition from energetic heavy ions to enhance formation of latent ion tracks. The average amorphous cross-section increases with the level of pre-damage and is linearly proportional to the electronic energy loss of the ions, with a slope dependent on the pre-damage level. For the highest energy ions (629 MeV Xe and 946 MeV Au), the tracks are continuous over the pre-damaged depth, but become discontinuous beyond the pre-damaged region. This work provides new understanding and insights on ion-solid interactions that significantly impact the interpretation of latent track formation processes, models of amorphization, and the fabrication of electro-ceramic devices.

Keywords: strontium titanate; Rutherford backscattering spectrometry/channeling; ion track; ion-beam processing; molecular dynamics

1. Introduction

Energetic heavy ions create highly defective or amorphous structures along their trajectories in various oxide ceramics [1, 2, 3, 4, 5, 6], which are known as latent ion tracks. The diameter of the ion tracks is typically on the scale of nanometers, and the track length can be tens of micrometers. Such an extremely large aspect ratio is very attractive to the fabrication of advanced nanostructures [7, 8, 9]. Physical properties, such as electronic conductivity [10, 11] and refractive index [12], of ion tracks vary significantly from those in the bulk, which can lead to new functionalities and applications in thin film devices. Latent ion tracks may be used as nano-channels for

electronic conductivity [13], and etched tracks have been used as templates for the growth of conductive nanowires in thin films [14]. Well-defined geometry and spatial distribution of the ion tracks are desired. However, this is a long-standing challenge because the intense far-from-equilibrium processes in ion-solid interactions remain poorly understood. For swift heavy ions (SHI), the electronic energy loss (dE/dx_{ele}) is several orders of magnitudes higher than the nuclear energy loss (dE/dx_{nucl}), and the energy deposition processes are dominated by inelastic interactions in the electronic subsystem. The dependence of ion track size (cross-section or diameter) on dE/dx_{ele} has been investigated by varying the atomic mass and energy of the incident ions [15, 16, 17, 18]. While research on tracks formed by SHI has been largely limited to accelerator facilities that can deliver heavy ions with energies from hundreds of MeV to GeV, recent studies have demonstrated track formation at tens of MeV [19].

As the energy deposited to electrons is further transferred from the electronic subsystem to the atomic subsystem by the electron-phonon (e-ph) interactions, a highly localized thermal spike is produced along the ion trajectory [20, 21, 22]. Defect formation, phase transitions and concentric strain can occur within the thermal spike when the electronic energy deposition exceeds a threshold value, which leads to observable latent track formation. For insulators such as SiO_2 and $LiNbO_3$ [5, 23, 24, 25, 26], ion tracks can be produced at relatively low (<10 keV nm^{-1}) values of dE/dx_{ele}. In contrast, much higher values of dE/dx_{ele} are required to form amorphous ion tracks in crystalline metallic materials [27, 28] and in semiconductors [29, 30]. Remarkable

variations of track formation threshold are also demonstrated for different phases. For example, ions with dE/dx_{ele} less than 15 keV nm^{-1} produce latent tracks in amorphous Ge [31]; however, crystalline Ge remains unaffected until dE/dx_{ele} increases to above 35 keV nm^{-1} [32]. The material-dependent variation of the threshold for track formation is not fully understood, but might be attributed to a reduced electron mean free path due to the structural imperfections. Our recent studies on single crystal $SrTiO_3$ have demonstrated that pre-existing crystalline disorder, such as from irradiation-induced defects, affects ion track formation [19, 33, 34, 35]. By employing 12 to 21 MeV ions, latent ion tracks are produced in defective $SrTiO_3$ with dE/dx_{ele} values above 6.7 keV nm^{-1} [35], which is significantly lower than the theoretically-predicted threshold of ~12.7 keV nm^{-1} [36] or the recently measured threshold of ~10 keV nm^{-1} [37] for pristine $SrTiO_3$. As shown by both molecular dynamics simulations [33] and experiments [35], the average amorphous track cross-section increases with increasing amount of pre-damage. In the present study, the synergy of electronic energy loss with pre-existing defects in $SrTiO_3$ is investigated over a much wider energy range (from 12 MeV up to 946 MeV) for different levels of pre-damage.

2. Experimental

The $SrTiO_3$ single crystals used in this study were (100) oriented, epi-polished (Ra and RMS surface roughness < 5 Å), 15×15×0.5 mm^3 wafers obtained from the MTI Corporation. No further surface preparation was performed. In order to produce a

pre-damaged state in the near-surface region, irradiations with 900 keV Au ions were performed using the 3 MV tandem accelerator and associated facilities in the Ion Beam Materials Laboratory (IBML) located at University of Tennessee (UT), Knoxville [38]. The ion flux was 4.2×10^{11} ions cm^{-2} s^{-1}, and ion fluences ranged from 4.4×10^{12} ions cm^{-2} to 4.6×10^{13} ions cm^{-2}. Different initial damage states were produced in multiple $SrTiO_3$ samples, and the disorder profiles were determined from Rutherford backscattering spectrometry in channeling geometry (RBS/C) using an iterative procedure previously described in detail for $SrTiO_3$ [39]. The peak fractional disorder levels of the different pre-damaged samples were ~0.01, 0.06, 0.10 and 0.21, where 0.0 refers to pristine $SrTiO_3$ and 1.0 refers to fully amorphous $SrTiO_3$.

One set of pre-damaged $SrTiO_3$ samples were irradiated using 21 MeV Ni, 21 MeV Cl, 20 MeV Ti and 12 MeV Ti ions in the IBML with an identical particle flux of 6.9×10^{10} ions cm^{-2} s^{-1}. The other set of pre-damaged samples were irradiated at the GSI Helmholtz Centre for Heavy Ion Research (Darmstadt, Germany) using 629 MeV Xe (4.8 MeV u^{-1}) to ion fluences of 1.0×10^{11} ions cm^{-2} and 1.0×10^{12} ions cm^{-2}, or using 946 MeV Au ions (4.8 MeV u^{-1}) to an ion fluence of 1.0×10^{11} ions cm^{-2}. The particle fluxes were 3.6×10^{8} ions cm^{-2} s^{-1} for the Xe irradiations and 2.5×10^{9} ions cm^{-2} s^{-1} for the Au irradiations. Pristine $SrTiO_3$ wafers were irradiated under identical conditions as references. The incident ion beams were at several degrees off the surface normal to avoid channeling effects. The stopping powers and ion ranges were predicted using the SRIM 2008 code [40] by employing full-cascade simulations. In

the SRIM simulations, the density of $SrTiO_3$ is 5.118 g cm^{-3}, and the displacement energies of Sr, Ti and O atoms are 80 eV [41], 70 eV [42] and 45 eV [42], respectively. The pre-damage from the 900 keV Au ions extends to a depth of about 250 nm. For the highest Au ion fluence (4.6×10^{13} cm^{-2}), the maximum concentration of implanted Au atoms is less than 0.006 at.% (<60 appm) at a depth of ~130 nm (see Fig. S1 in Supplementary Material). Chemical effects and lattice distortion due to the implanted Au atoms are expected to be negligible, compared to the much higher concentration of irradiation-induced defects. The penetration depths for the high energy ion are much larger, e.g., more than several μm (i.e., 12 MeV Ti) or several tens of μm (i.e., 629 MeV Xe). Consequently, the high energy ions are deposited well beyond the pre-damaged region and do not contribute to any observed effect in this region.

Following the SHI and lower energy irradiations, RBS/C measurements employing 3.5 MeV He ions were performed using the IBML facilities at UT to characterize damage evolution. The ion irradiations and ion beam analysis were performed at room temperature in high vacuum (<2.0×10^{-7} Torr). Beam heating effects were negligible during the ion irradiations.

The pristine and pre-damaged $SrTiO_3$ samples irradiated with 629 MeV Xe ions were also characterized using a 5^{th} order aberration corrected Nion UltraSTEM200 scanning transmission electron microscope (STEM) operating at 200 kV at Oak Ridge National Laboratory. The electron probe current used for imaging in the experiment

was 28±2 pA. Annular bright field (ABF) imaging was done with the collection semi-angles between 15-28 mrad. No evidence for electron beam induced recrystallization of the amorphous tracks was observed during the STEM characterization.

3. Thermal spike model

Molecular dynamics (MD) simulations of 629 MeV Xe ion irradiation of pristine and pre-damaged $SrTiO_3$ were performed in order to confirm the synergistic interaction of pre-existing defects with the electronic energy loss. The energy deposition from the hot electrons to the lattice atoms can be obtained by using the inelastic thermal spike (iTS) model [22]. In the iTS model, energy exchange between the electronic and the atomic subsystems is described via a set of two heat diffusion equations (eqs. 1 and 2), which describe the electronic temperature T_e and the atomic temperature T_α evolution and are given by:

$$C_e(T_e)\frac{\partial T_e}{\partial t} = \frac{1}{r}\frac{\partial}{\partial r}\left[r\,K_e(T_e)\frac{\partial T_e}{\partial r}\right] - g(T_e - T_a) + A(r,t) \quad (1)$$

$$C_a(T_a)\frac{\partial T_a}{\partial t} = \frac{1}{r}\frac{\partial}{\partial r}\left[r\,K_a(T_a)\frac{\partial T_a}{\partial r}\right] + g(T_e - T_a) \quad (2)$$

where C_e and C_α are the heat capacities of the electronic and the atomic systems; K_e and K_α are the electronic and lattice thermal conductivities, respectively; and g is the e-ph coupling parameter. The term $A(r, t)$ describes the spatial and temporal energy deposition from the incident ion to the electrons [43]. The electronic specific heat C_e

is 1 J cm^{-3} K^{-1} [22, 44] and the specific heat of the lattice C_a is 0.544 J cm^{-3} K^{-1} [45]. K_e is equal to $C_e D_e$ [22, 44], where D_e is the thermal diffusivity and has a value of 1.0 cm^2 s^{-1} [22, 44], and K_α is 11.2 W m^{-1} K^{-1} at 300 K. The e-ph coupling parameter g is equal to K_e/λ^2 [22], where λ is the e-ph mean free path; for the pristine crystalline system, it is 4.7 nm [22, 46]. For the system with pre-existing defects, as described previously [19, 33], K_e and K_α are each reduced by an order of magnitude, and a reduced value of λ=3.0 nm is used. The electronic energy loss for a 629 MeV Xe ion in $SrTiO_3$ was calculated using the SRIM code. The calculated energy deposition profiles for a pristine crystalline and a pre-damaged $SrTiO_3$ system are shown in Fig. 1, which were used as input in the MD simulations.

The MD simulations were performed using the DL_POLY code [47] and the McCoy et al. empirical potential [48], joined with the short-range ZBL potential [49]. The ZBL potential was used for all pair interactions. The simulation cell consisted of 936,000 atoms, the size of the cell was 470 Å×470 Å×51 Å under periodic boundary conditions. The pre-damaged system contained 1.5 % Frenkel pairs (FP), which were randomly introduced in the system. This pre-damaged system was previously found to predict track sizes due to 21 MeV Ni ions in good agreement with those measured experimentally for a pre-damaged disorder level of 0.07 [19], similar to experimental disorder levels in the present study. Both the pristine and the pre-damaged systems were equilibrated at 300 K under the constant-pressure and temperature (NPT) ensemble using a 1 fs timestep prior to irradiation. The irradiation simulations were

performed under the constant-volume, constant-energy (NVE) ensemble at 300 K, along the z direction, using a variable timestep. The velocities of the atoms within 10 Å from the MD box boundaries along the x and y dimensions are connected to a Langevin thermostat with 300 K temperature, to emulate the energy dissipation in the bulk.

4. Results and discussion

The RBS/C spectra of the SHI irradiated pristine and defective single crystal $SrTiO_3$ are shown in Fig. 2a and 2b, respectively. The SHI irradiations of the pre-damaged samples (the star patterns, Fig. 2b) lead to a rapid increase in backscattering yields at low ion fluences that indicate direct impact amorphization along the ion path. The dE/dx_{ele} and dE/dx_{nucl} of the intermediate energy and swift heavy ions used in the present study are provided in Table 1, along with the ratio of $(dE/dx_{ele})/(dE/dx_{nucl})$ predicted by the SRIM code at the depth of the pre-damage peak (~100 nm). For the SHI, the stopping powers and their ratio at 1 μm are also included. In the case of the swift heavy ions, the dE/dx_{ele} is above the track formation threshold of ~10 keV nm^{-1} [37], while dE/dx_{nucl} is negligible. The damage accumulation is dominated by the production of amorphous ion tracks due to the electronic energy deposition. As shown in Table 1, the dE/dx_{ele} and dE/dx_{nucl} values for SHI are essentially constant over the first 1 μm of depth from the surface, and the average amorphous cross-section of the ion tracks should be invariant, which is evident by the linear increase in backscattering yields as a function of channel number (for Sr sublattice, 1120 is 1 μm

of depth from the surface) [50], as shown in Fig. 2a. The irradiation-induced fractional disorder due to SHI in the pristine $SrTiO_3$ is quantified by the ratio, r, of the relative backscattering yield to the amorphous level: $r = (\chi_d-\chi_r) / (\chi_a-\chi_r)$, where χ_d, χ_r and χ_a are the backscattering yields at 100 nm (channel number ~1460) in the irradiated region, in the pristine reference sample without ion irradiation and in amorphous $SrTiO_3$, respectively. As the fluence of 629 MeV Xe ions (dE/dx_{ele}=29.0 keV nm^{-1}) increases from 1.0×10^{11} to 1.0×10^{12} cm^{-2}, an elevated production and density of ion tracks leads to a proportionally increased value of r (from 0.8% to 7.4%). For the 946 MeV Au ion irradiations, the value of r (2.7%) is higher than that for Xe (0.8%) for an identical ion fluence of 1.0×10^{11} cm^{-2}, which is attributed to the higher dE/dx_{ele} (39.8 keV nm^{-1}) for the Au ions.

For the 900 keV Au ions, dE/dx_{ele} is comparable to dE/dx_{nucl} (Table 1), and it is far below the threshold for formation of ion tracks. The ballistic displacements of lattice nuclei due to dE/dx_{nucl} dominate the damage accumulation processes. From the surface to a depth of ~250 nm, pre-damage states with a peak distribution are created, as shown in Fig. 2b with r of 6.7%. The SHI irradiations produce ion tracks in the pre-damaged regions near the surface and in the pristine regions. Within the pre-damaged layer, the backscattering yield increases rapidly. As indicated in Fig. 2b, Xe and Au irradiations to an ion fluence of 1.0×10^{11} cm^{-2} increase r by 3.3% (from 6.7% to 9.9%) and 6.0% (from 6.7% to 12.7%) in the pre-damaged regions, compared to 0.8% and 2.7% in the pristine regions (Fig. 2a), respectively. The ratio r increases

dramatically by 34.7% (from 6.7% to 41.4%) after Xe irradiation to an ion fluence of 1.0×10^{12} cm^{-2}, which suggests that substantially more damage is produced in the defective lattice than in the pristine region (7.4%). The differences in the damage accumulation suggest that the amorphous tracks are not spatially homogeneous along the ion trajectories. In the pre-damaged regions, the average amorphous cross-sections are larger, but decrease substantially in the pristine regions beneath the pre-damage states.

In order to quantitatively correlate the enhanced ion track formation with the pre-existing defects, the net increase of the backscattering yield at channel number *n* ($\chi(n)_{net}$) in the RBS/C spectra is calculated based on the expression:

$$\chi(n)_{net} = \chi(n)_{df} - \chi(n)_{ps} + \chi(n)_{vg} \quad (3)$$

Where $\chi(n)_{vg}$, $\chi(n)_{ps}$ and $\chi(n)_{df}$ are the channeling backscattering yields collected on a reference virgin (unirradiated) sample, on a pristine region that experienced only SHI irradiation, and on a defective region irradiated by both 900 keV Au ions and SHI, respectively. An iterative procedure [39] was applied to $\chi(n)_{net}$ to extract the dechanneling fraction and determine the relative disorder as a function of depth. The results are shown in Fig. 3a-3f as a function of depth for different irradiation conditions and histories. Because the linear increase in backscattering yield ($\chi(n)_{ps}$), which was shown in Fig. 2a, has already been extracted before the iterative procedure

was applied, the relative disorder profiles shown in Fig. 3 do not include the background disorder equivalent to SHI tracks in pristine material. For a low initial damage of ~0.01 (Fig. 3a), irradiation with 629 MeV Xe to an ion fluence of 1.0×10^{11} cm^{-2} leads to insignificant increase in the initial damage profile, and the scatter in the data is attributed to the statistics of backscattering yields and the resolution of RBS/C characterization. After Xe irradiation to an ion fluence of 1.0×10^{12} cm^{-2}, the relative disorder increases significantly from ~0.01 to 0.075 (+~650%). As shown in Fig. 3b, for an initial disorder level of 0.06, the Xe irradiations raise the relative disorder to 0.08 (+30%) for an ion fluence of 1.0×10^{11} cm^{-2} and to 0.32 (+430%) for an ion fluence of 1.0×10^{12} cm^{-2}. Further increase of the initial damage levels results in larger amorphous cross-sections, and damage accumulation rate decreases due to amorphous track overlapping, as the relative disorder approaches the amorphous level (1.0). For example, for an initial damage level of 0.21 (Fig. 3c), the relative disorder increases to 0.32 (+54%) and 0.81 (+300%) after Xe irradiation to ion fluences of 1.0×10^{11} and 1.0×10^{12} cm^{-2}, respectively. A similar trend is observed for the 946 MeV Au irradiations, as shown in Fig. 3d-3f. After irradiated to an ion fluence of 1.0×10^{11} cm^{-2}, the relative disorder increases from ~0.01 to 0.02 (+~100%), from 0.06 to 0.10 (+67%), and from 0.10 to 0.24 (+140%), respectively. A more efficient damage accumulation under Au irradiation indicates a larger track size in the pre-damaged regions.

During SHI irradiations, ion track formation is governed by electronic energy

deposition from the ions and the subsequent energy dissipation to the lattice of the target material. It is important to note that the pre-damaged layers are not heavily disordered and the relatively damage levels (maximum 0.21) are far from amorphous. No significant volume swelling nor decrease of atomic density, such as in highly disordered or amorphized crystals [51, 52], are expected. Therefore, the density of the target electrons in the pre-damaged layers should not vary from that in the pristine region. As the result, the electronic energy loss per unit volume, which is determined by the electron-electron interactions between the SHI and the target atoms, is not modified by the pre-damage. However, the electronic energy dissipation processes and energy transfer from the electronic subsystem to the atomic subsystem are sensitive to small amounts of lattice imperfections. The low energy irradiations create point defects and defect clusters that act as scattering centers, which can result in considerable reduction of the electron mean free path [53] and decrease in thermal conductivity [54]. The e-ph coupling is enhanced, and at the same time, the energy dissipation processes are obstructed. The energy deposition profiles to the electronic to the atomic subsystem have been calculated, as shown in Fig. 1, for a pristine crystal and a pre-damaged crystal with decreased thermal conductivities. Within the thermal spike, the energy deposition density to the atomic subsystem is enhanced by the pre-damaged states. MD simulations have been performed using the corresponding energy deposition profiles for both the pristine crystal and the pre-damaged crystal, and the spatial distributions of damage induced by 629 MeV Xe ions are shown in Fig. 4. For the pristine crystal, the energy transferred from a single ion is not sufficient to

create a continuous track in the simulation cell. However, by performing simulations of four consecutive ions (inelastic thermal spikes), the fourth ion finally results in the formation of an amorphous latent track with a diameter varying from 1 to 2.4 nm, as shown in Fig. 4a and 4b. In these simulations, the interval between ion events is 20 ps, and the ion trajectories were separated by 2 to 4 nm. While there was partial overlap of the affected thermal spike volumes, these results clearly demonstrate the resistance of pristine $SrTiO_3$ to amorphous track formation, which is consistent with the experimental observations, discussed below, of discontinuous track formation in pristine $SrTiO_3$. In the pre-damaged region, the atomic defects act synergistically with the electronic energy loss [19, 33, 34, 35], and a larger amorphous ion track with a diameter of 5.2 ± 0.4 nm is formed by a single ion, as shown in Fig. 4c and 4d. As previously demonstrated [19, 35], the dependence of track size on pre-damage level is determined experimentally from the disorder profiles in Fig. 3 by employing the direct impact model [55, 56] to fit the change in disorder with ion fluence at a constant depth. In this model, the amorphous fraction from track formation, f_a, is given by:

$$f_a = 1 - (1 - f_0) \cdot \exp(-(\sigma_a - \sigma_p) \cdot \Phi) \quad (4)$$

where σ_a is the actual average amorphous cross-section of the latent tracks in the pre-damaged region at a specific depth (peak disorder), σ_p is the average cross-section of latent tracks in pristine $SrTiO_3$ (this was subtracted in the RBS/C analysis), Φ is the

ion fluence, and f_0 is the relative disorder fraction of the initial pre-damage state. The value of σ_p is estimated by applying the direct impact model to the ratio, r (defined earlier), for SHI in pristine $SrTiO_3$:

$$r = 1 - \exp(-\sigma_p \cdot \Phi) \quad (5)$$

The values for σ_a are summarized in Table 2 for the two different SHIs and initial disorder levels. For a low initial damage level, the experimentally determined track sizes are consistent with the MD simulations (1.5% FP). The amorphous cross-sections for the SHI exhibit a monotonic increase as a function of initial damage, which agrees with the studies using intermediated energy ions [19, 35]. A synergy between the defects created by 900 keV Au and the dE/dx_{ele} of the SHI promotes the formation of latent ion tracks in defective $SrTiO_3$. The average amorphous cross-section of the ion tracks increases with increasing dE/dx_{ele} (Table 2). The dependence of ion track size on electronic energy loss is shown in Fig. 5; also included for comparison are the track sizes determined under similar pre-damaged conditions for 21 MeV Ni, 21 MeV Cl, 20 MeV Ti and 12 MeV Ti ions, as well as the average track sizes for SHI in pristine $SrTiO_3$. Clear evidence of a synergistic effect and linear dependence of amorphous cross-section on electronic stopping power are revealed. The threshold for synergistic track formation is estimated to be about 7 keV nm^{-1} for initial disorder levels between 0.06 and 0.15, which agrees with the prediction at intermediate energies [35]. In the case of pristine $SrTiO_3$, the results in

Fig. 5 clearly demonstrate smaller average track sizes. The results further suggest that this synergistic track formation is enhanced by higher initial damage levels, which agrees with the results summarized in Table 2 and previous MD simulations [33].

According to the results shown in Fig. 5, it is expected that by choosing appropriate combinations of pre-damage state with the dE/dx_{ele} for an ion, one may modify the geometry of ion tracks at designated depths in crystalline $SrTiO_3$ and introduce well-defined amorphous domains in thin films of $SrTiO_3$ that are embedded in multi-layer structures. Another beneficial impact from the synergistic effect is that as the average amorphous cross-section increases, the continuity of the latent ion tracks is improved. It has been a critical issue for the studies and applications that SHI tracks are discontinuous in some target materials even for high values of dE/dx_{ele} [11, 32, 57, 58], which is also evident in the ABF image shown in Fig. 6a. The cross-sectional STEM image shows ion tracks formed in the pre-damaged $SrTiO_3$ after irradiation with 629 MeV Xe ions to a fluence of 1.0×10^{11} cm^{-2}. The pre-damaged region predominantly exists within ~200 nm from the irradiated surface, and continuous ion tracks are only found within this depth region. In contrast, at depths beyond the pre-damaged region (i.e., pristine structure), the ion tracks become smaller and discontinuous (Fig. 6a). The observation of continuous track formation in the pre-damaged $SrTiO_3$ is consistent with the predictions from MD simulations and RBS measurements. A cross-sectional ABF image of a single ion track formed in the pre-damaged region by a 629 MeV Xe ion is shown in Fig. 6b. It demonstrates that

the amorphous ion track formed in the pre-damage region with a relative disorder of 0.10 (according to RBS/C result) is continuous in nature. The diameter of this ion track is measured to be ~8.4 nm, which is slightly smaller than that determined from the RBS/C results (~11.9 nm) if a circular cross-section is assumed. The difference may be explained by statistical deviation from the average diameter (RBS/C result), and could be attributed to the strain fields at the amorphous-crystalline interface that leads to dechanneling of the He ions in the RBS/C measurements. In addition, the 8.4 nm amorphous track viewed by cross-sectional STEM is embedded in a thin crystalline region of $SrTiO_3$ (~ 30 nm sample thickness), and the full diametrical extent of the amorphous track may not be resolvable due to the high crystalline/amorphous ratio at the track periphery. The idea of enhancing the continuity of latent tracks by introducing low concentrations of defects is very attractive. It is known that the defects induced by elastic scattering events (pre-damage) can be removed by post-treatments, such as thermal or electron-beam annealing processes [59, 60, 61]; while at the same time, the continuous amorphous ion tracks survive recrystallization due to much higher activation energies.

5. Conclusions

The morphology of latent ion tracks produced by energetic heavy ions in single crystal $SrTiO_3$ is dependent on the magnitude of the electronic energy loss, the presence of pre-existing damage states, and the amount of pre-existing damage. The high density of electronic energy loss by the ions results in a local thermal spike, via

electron-phonon coupling, along the ion trajectory. The presence of pre-existing defects decreases the electronic and atomic thermal conductivities and increase the electron-phonon coupling, which increases the intensity and radial confinement of the thermal spike. Above a threshold electronic energy loss of about 7 keV/nm, amorphous latent tracks are produced for pre-existing fraction disorder above 0.06 due to a local melt and quench process. Amorphous track size increases with electronic energy loss and the amount of initial disorder. While latent tracks are not produced in pristine $SrTiO_3$ by energetic ions up to 21 MeV Ni, swift heavy ions (629 MeV Xe and 946 MeV Au ions) produce discontinuous tracks in pristine $SrTiO_3$ and much larger continuous track in pre-damage crystals. The change in ion track morphology for SHI from continuous in the pre-damaged region to discontinuous in the pristine crystal beyond the pre-damaged depth has been confirmed by STEM characterization and MD simulations. This synergy between pre-existing defects and electronic energy loss could be combined with the excellent penetration capability of energetic heavy ions to produce nanoscale cylindrical structures of varying sizes in single crystals, thin films and multi-layered structures. Amorphous track formation is significantly enhanced by the coupling of highly ionizing ions with pre-existing damage, and similar enhancement of damage production may occur in other materials at intermediate energies, where electronic and nuclear energy loss are comparable. The lifetime and performance of materials used in harsh radiation environments may be affected by these synergistic processes.

Acknowledgements

This work was supported by the U.S. Department of Energy, Office of Science, Basic Energy Sciences, Materials Sciences and Engineering Division. Haizhou Xue was supported by the University of Tennessee Governor's Chair program.

References

[1] E. Silk and R. Barnes, Examination of fission fragment tracks with an electron microscope. Philosophical Magazine 4 (1959) 970-972.

[2] A. Meftah, F. Brisard, J. Costantini, M. Hage-Ali, J. Stoquert, F. Studer and M. Toulemonde, Swift heavy ions in magnetic insulators: A damage-cross-section velocity effect. Physical Review B 48 (1993) 920.

[3] W. Wesch, A. Kamarou and E. Wendler, Effect of high electronic energy deposition in semiconductors. Nuclear Instruments and Methods in Physics Research Section B: Beam Interactions with Materials and Atoms 225 (2004) 111-128.

[4] C. Dufour, A. Audouard, F. Beuneu, J. Dural, J. Girard, A. Hairie, M. Levalois, E. Paumier and M. Toulemonde, A high-resistivity phase induced by swift heavy-ion irradiation of Bi: a probe for thermal spike damage? Journal of Physics: Condensed Matter 5 (1993) 4573.

[5] P. Kluth, C. Schnohr, O. Pakarinen, F. Djurabekova, D. Sprouster, R. Giulian, M. C. Ridgway, A. Byrne, C. Trautmann and D. Cookson, Fine structure in swift heavy ion tracks in amorphous SiO_2. Physical review letters 101 (2008) 175503.

[6] M. C. Ridgway, T. Bierschenk, R. Giulian, B. Afra, M. Rodriguez, L. L. Araújo, A. Byrne, N. Kirby, O. Pakarinen and F. Djurabekova, Tracks and voids in amorphous Ge induced by swift heavy-ion irradiation. Physical review letters 110 (2013) 245502.

[7] M. Toulemonde, C. Trautmann, E. Balanzat, K. Hjort and A. Weidinger, Track formation and fabrication of nanostructures with MeV-ion beams. Nuclear Instruments and Methods in Physics Research Section B: Beam Interactions with Materials and Atoms 216 (2004) 1-8.

[8] M. T. Molares, V. Buschmann, D. Dobrev, R. Neumann, R. Scholz, I. U. Schuchert and J. Vetter, Single-crystalline copper nanowires produced by electrochemical deposition in polymeric ion track membranes. Adv. Mater 13 (2001) 62-65.

[9] F. Bergamini, M. Bianconi and S. Cristiani, Wet and vapor etching of tracks produced in SiO_2 by Ti ion irradiation. Nuclear Instruments and Methods in Physics Research Section B: Beam Interactions with Materials and Atoms 257 (2007) 593-596.

[10] J.-H. Zollondz and A. Weidinger, Towards new applications of ion tracks. Nuclear Instruments and Methods in Physics Research Section B: Beam Interactions with Materials and Atoms 225 (2004) 178-183.

[11] S. Gupta, H. Gehrke, J. Krauser, C. Trautmann, D. Severin, M. Bender, H. Rothard and H. Hofsäss, Conducting ion tracks generated by charge-selected swift heavy ions. Nuclear Instruments and Methods in Physics Research Section B: Beam Interactions with Materials and Atoms 381 (2016) 76-83.

[12] A. García-Navarro, J. Olivares, G. García, F. Agulló-López, S. García-Blanco, C. Merchant and J. S. Aitchison, Fabrication of optical waveguides in KGW by swift heavy ion beam irradiation. Nuclear Instruments and Methods in Physics Research Section B: Beam Interactions with Materials and Atoms 249 (2006) 177-180.

[13] M. Waiblinger, C. Sommerhalter, B. Pietzak, J. Krauser, B. Mertesacker, M. C. Lux-Steiner, S. Klaumünzer, A. Weidinger, C. Ronning and H. Hofsäß, Electrically conducting ion tracks in diamond-like carbon films for field emission. Applied Physics A: Materials Science & Processing 69 (1999) 239-240.

[14] I. Enculescu, Z. Siwy, D. Dobrev, C. Trautmann, M. Toimil Molares, R. Neumann, K. Hjort, L. Westerberg and R. Spohr, Copper nanowires electrodeposited in etched single-ion track templates. Applied Physics A: Materials Science & Processing 77 (2003) 751-755.

[15] M. Toulemonde, E. Balanzat, S. Bouffard and J. Jousset, Structural modifications induced by electronic energy deposition during the slowing down of heavy ions in matter. Nuclear Instruments and Methods in Physics Research Section B: Beam Interactions with Materials and Atoms 39 (1989) 1-6.

[16] N. Ishikawa, T. Sonoda, T. Sawabe, H. Sugai and M. Sataka, Electronic stopping power dependence of ion-track size in UO_2 irradiated with heavy ions in the energy range of~ 1MeV/u. Nuclear Instruments and Methods in Physics Research Section B: Beam Interactions with Materials and Atoms 314 (2013) 180-184.

[17] D. Schauries, B. Afra, T. Bierschenk, M. Lang, M. Rodriguez, C. Trautmann, W. Li, R. Ewing and P. Kluth, The shape of ion tracks in natural apatite. Nuclear Instruments and Methods in Physics Research Section B: Beam Interactions with Materials and Atoms 326 (2014) 117-120.

[18] H. Vázquez, E. Åhlgren, O. Ochedowski, A. Leino, R. Mirzayev, R. Kozubek, H. Lebius, M. Karlušic, M. Jakšic and A. Krasheninnikov, Creating nanoporous graphene with swift heavy ions. Carbon 114 (2017) 511-518.

[19] W. J. Weber, E. Zarkadoula, O. H. Pakarinen, R. Sachan, M. F. Chisholm, P. Liu, H. Xue, K. Jin and Y. Zhang, Synergy of elastic and inelastic energy loss on ion track formation in $SrTiO_3$. Scientific reports 5 (2015) 7726.

[20] A. Meftah, F. Brisard, J. Costantini, E. Dooryhee, M. Hage-Ali, M. Hervieu, J. Stoquert, F. Studer and M. Toulemonde, Track formation in SiO_2 quartz and the thermal-spike mechanism. Physical Review B 49 (1994) 12457.

[21] M. Toulemonde, J. Costantini, C. Dufour, A. Meftah, E. Paumier and F. Studer, Track creation in SiO_2 and $BaFe_{12}O_{19}$ by swift heavy ions: a thermal spike description. Nuclear Instruments and Methods in Physics Research Section B: Beam Interactions with Materials and Atoms 116 (1996) 37-42.

[22] M. Toulemonde, W. Assmann, C. Dufour, A. Meftah, F. Studer and C. Trautmann, Experimental phenomena and thermal spike model description of ion tracks in amorphisable inorganic insulators. Mat. Fys. Medd. Dan. Vid. Selsk 52 (2006) 263.

[23] M. Toulemonde, W. J. Weber, G. Li, V. Shutthanandan, P. Kluth, T. Yang, Y. Wang and Y. Zhang, Synergy of nuclear and electronic energy losses in ion-irradiation processes: The case of vitreous silicon dioxide. Physical Review B 83 (2011) 054106.

[24] G. Szenes, Amorphous track formation in SiO_2. Nuclear Instruments and Methods in Physics Research Section B: Beam Interactions with Materials and Atoms 122 (1997) 530-533.

[25] J. Olivares, G. García, F. Agulló-López, F. Agulló-Rueda, J. Soares and A. Kling, Optical investigation of the propagation of the amorphous–crystalline boundary in ion-beam irradiated $LiNbO_3$. Nuclear Instruments and Methods in Physics Research Section B: Beam Interactions with Materials and Atoms 242 (2006) 534-537.

[26] R. Sachan, O. Pakarinen, P. Liu, M. Patel, M. Chisholm, Y. Zhang, X. Wang and W. Weber, Structure and band gap determination of irradiation-induced amorphous nano-channels in $LiNbO_3$. Journal of Applied Physics 117 (2015) 135902.

[27] Z. Wang, C. Dufour, E. Paumier and M. Toulemonde, The Se sensitivity of metals under swift-heavy-ion irradiation: a transient thermal process. Journal of Physics: Condensed Matter 6 (1994) 6733.

[28] A. Audouard, E. Balanzat, S. Bouffard, J. Jousset, A. Chamberod, A. Dunlop, D. Lesueur, G. Fuchs, R. Spohr and J. Vetter, Evidence for amorphization of a metallic alloy by ion electronic energy loss. Physical review letters 65 (1990) 875.

[29] M. Levalois, P. Bogdanski and M. Toulemonde, Induced damage by high energy heavy ion irradiation at the GANIL accelerator in semiconductor materials. Nuclear Instruments and Methods in Physics Research Section B: Beam Interactions with Materials and Atoms 63 (1992) 14-20.

[30] G. Szenes, Z. Horvath, B. Pecz, F. Paszti and L. Toth, Tracks induced by swift heavy ions in semiconductors. Physical Review B 65 (2002) 045206.

[31] T. Steinbach, C. Schnohr, P. Kluth, R. Giulian, L. Araujo, D. Sprouster, M. C. Ridgway and W. Wesch, Influence of electronic energy deposition on the structural modification of swift heavy-ion-irradiated amorphous germanium layers. Physical Review B 83 (2011) 054113.

[32] A. Colder, O. Marty, B. Canut, M. Levalois, P. Marie, X. Portier, S. Ramos and M. Toulemonde, Latent track formation in germanium irradiated with 20, 30 and 40 MeV fullerenes in the electronic regime. Nuclear Instruments and Methods in Physics Research Section B: Beam Interactions with Materials and Atoms 174 (2001) 491-498.

[33] E. Zarkadoula, O. H. Pakarinen, H. Xue, Y. Zhang and W. J. Weber, Predictive modeling of synergistic effects in nanoscale ion track formation. Physical Chemistry Chemical Physics 17 (2015) 22538-22542.

[34] E. Zarkadoula, H. Xue, Y. Zhang and W. J. Weber, Synergy of inelastic and elastic energy loss: Temperature effects and electronic stopping power dependence. Scripta Materialia 110 (2016) 2-5.

[35] H. Xue, E. Zarkadoula, P. Liu, K. Jin, Y. Zhang and W. J. Weber, Amorphization due to electronic energy deposition in defective strontium titanate. Acta Materialia 127 (2017) 400-406.

[36] M. Karlusić, S. Akcöltekin, O. Osmani, I. Monnet, H. Lebius, M. Jaksić and M. Schleberger, Energy threshold for the creation of nanodots on SrTiO3 by swift heavy ions. New Journal of Physics 12 (2010) 043009.

[37] M. Karlušić, M. Jakšić, H. Lebius, B. Ban-d'Etat, R. Wilhelm, R. Heller and M. Schleberger, Swift

heavy ion track formation in $SrTiO_3$ and TiO_2 under random, channeling and near-channeling conditions. Journal of Physics D: Applied Physics 50 (2017) 205302.

[38] Y. Zhang, M. L. Crespillo, H. Xue, K. Jin, C.-H. Chen, C. L. Fontana, J. Graham and W. J. Weber, New ion beam materials laboratory for materials modification and irradiation effects research. Nuclear Instruments and Methods in Physics Research Section B: Beam Interactions with Materials and Atoms 338 (2014) 19-30.

[39] Y. Zhang, J. Lian, Z. Zhu, W. D. Bennett, L. V. Saraf, J. L. Rausch, C. A. Hendricks, R. Ewing and W. J. Weber, Response of strontium titanate to ion and electron irradiation. Journal of Nuclear Materials 389 (2009) 303-310.

[40] J. F. Ziegler, M. D. Ziegler and J. P. Biersack (2008). *SRIM: the stopping and range of ions in matter*. Cadence Design Systems.

[41] K. L. Smith, M. Colella, R. Cooper and E. R. Vance, Measured displacement energies of oxygen ions in titanates and zirconates. Journal of nuclear materials 321 (2003) 19-28.

[42] K. L. Smith and N. J. Zaluzec, The displacement energies of cations in perovskite ($CaTiO_3$). Journal of nuclear materials 336 (2005) 261-266.

[43] M. Waligorski, R. Hamm and R. Katz, The radial distribution of dose around the path of a heavy ion in liquid water. International Journal of Radiation Applications and Instrumentation. Part D. Nuclear Tracks and Radiation Measurements 11 (1986) 309-319.

[44] A. Meftah, J. Costantini, N. Khalfaoui, S. Boudjadar, J. Stoquert, F. Studer and M. Toulemonde, Experimental determination of track cross-section in $Gd_3Ga_5O_2$ and comparison to the inelastic thermal spike model applied to several materials. Nuclear Instruments and Methods in Physics Research Section B: Beam Interactions with Materials and Atoms 237 (2005) 563-574.

[45] http://www.toplent.com/SrTiO3.htm.

[46] C. Dufour, V. Khomrenkov, Y. Wang, Z. Wang, F. Aumayr and M. Toulemonde, An attempt to apply the inelastic thermal spike model to surface modifications of CaF_2 induced by highly charged ions: comparison to swift heavy ions effects and extension to some others material. Journal of Physics: Condensed Matter 29 (2017) 095001.

[47] I. T. Todorov, W. Smith, K. Trachenko and M. T. Dove, DL_POLY_3: new dimensions in molecular dynamics simulations via massive parallelism. Journal of Materials Chemistry 16 (2006) 1911-1918.

[48] M. A. Mccoy, R. W. Grimes and W. E. Lee, Phase stability and interfacial structures in the SrO–$SrTiO_3$ system. Philosophical Magazine A 75 (1997) 833-846.

[49] J. F. Ziegler, J. Biersack and U. Littmark, The stopping and range of ions in matter, Vol. 1. 1, Pergamon Press, New York(1985).

[50] O. Herre, W. Wesch, E. Wendler, P. Gaiduk, F. Komarov, S. Klaumünzer and P. Meier, Formation of discontinuous tracks in single-crystalline InP by 250-MeV Xe-ion irradiation. Physical Review B 58 (1998) 4832.

[51] C. Trautmann, M. Boccanfuso, A. Benyagoub, S. Klaumunzer, K. Schwartz and M. Toulemonde, Swelling of insulators induced by swift heavy ions. Nucl. Instrum. Methods Phys. Res. Sect. B-Beam Interact. Mater. Atoms 191 (2002) 144-148.

[52] Y. Katoh, H. Kishimoto and A. Kohyama, Low temperature swelling in beta-SiC associated with point defect accumulation. Materials Transactions 43 (2002) 612-616.

[53] W. Kang, B. Kang, Q. Chen, J. Wu, Y. Bai, W. Chu, D. Christen, R. Kerchner and S.-I. Lee, Triple sign reversal of the Hall effect in $HgBa_2CaCu_2O_6$ thin films after heavy-ion irradiation. Physical Review B 61 (2000) 722.

[54] C. Yu, M. L. Scullin, M. Huijben, R. Ramesh and A. Majumdar, Thermal conductivity reduction in oxygen-deficient strontium titanates. Applied Physics Letters 92 (2008) 191911.

[55] J. F. Gibbons, Ion implantation in semiconductors—Part II: Damage production and annealing. Proceedings of the IEEE 60 (1972) 1062-1096.

[56] W. Weber, Models and mechanisms of irradiation-induced amorphization in ceramics. Nuclear Instruments and Methods in Physics Research Section B: Beam Interactions with Materials and Atoms 166 (2000) 98-106.

[57] E. Dartyge, J. Duraud, Y. Langevin and M. Maurette, New model of nuclear particle tracks in dielectric minerals. Physical Review B 23 (1981) 5213.

[58] P. Gaiduk, A. N. Larsen, C. Trautmann and M. Toulemonde, Discontinuous tracks in arsenic-doped crystalline $Si_{0.5}Ge_{0.5}$ alloy layers. Physical Review B 66 (2002) 045316.

[59] E. Wendler, A. Heft and W. Wesch, Ion-beam induced damage and annealing behaviour in SiC. Nuclear Instruments and Methods in Physics Research Section B: Beam Interactions with Materials and Atoms 141 (1998) 105-117.

[60] Y. Zhang, J. Lian, C. M. Wang, W. Jiang, R. C. Ewing and W. J. Weber, Ion-induced damage accumulation and electron-beam-enhanced recrystallization in $SrTiO_3$. Physical Review B 72 (2005) 094112.

[61] Y. Zhang, R. Sachan, O. H. Pakarinen, M. F. Chisholm, P. Liu, H. Xue and W. J. Weber, Ionization-induced annealing of pre-existing defects in silicon carbide. Nature communications 6 (2015) 8049.

Table 1.

Ion	Au		Xe	Ni	Cl	Ti	
E_{ion} (MeV)	0.9	946	629	21	21	20	12
dE/dx_{ele}	0.85	39.8	29.0	9.9	7.5	8.6	7.1
		(39.8)	(29.0)				
dE/dx_{nucl}	0.45	0.006	0.002	0.084	0.019	0.050	0.080
		(0.006)	(0.002)				
Ratio	1.9	$>6\times10^3$	$>1\times10^4$	118	394	172	89

Table 1. The electronic and nuclear stopping powers (in keV nm^{-1}) and the ratio of electronic to nuclear stopping powers in $SrTiO_3$ for the ions used in this study at the depth of the pre-damage peak (100 nm). For the SHI, the stopping powers and ratios at 1 μm are included in brackets.

Table 2.

Initial disorder level	629 MeV Xe		946 MeV Au	
	Amorphous cross-section (nm^2)	Track diameter (nm)	Amorphous cross-section (nm^2)	Track diameter (nm)
0.00*	7.6±0.8	3.1±0.3	27.3 ± 2.7	5.9 ± 0.6
0.01	14.3±2.1	4.3±0.6	31.4 ± 4.7	6.3 ± 0.9
0.06	39.8 ± 6.8	7.1 ± 1.1	76.5 ± 11.5	9.9 ± 1.0
0.10	112.6 ± 16.9	12.0 ± 1.8	197.4 ± 29.6	15.8 ± 2.4
0.10 (STEM)		~8.4		
0.21	124.8 ± 18.7	12.6 ± 1.9		
FP 1.5% (MD)		5.2 ± 0.4		

Table 2. The average amorphous cross-sections and track diameters, as determined by the direct-impact model, for different combinations of initial disorder level and ions. The fitting error and the experiment uncertainty (15%) have been considered. The results of MD simulation for a Frenkel pair concentration of 1.5%, and STEM characterization for a pre-damage level of ~0.10 are included.

* Pristine condition

Figure 1

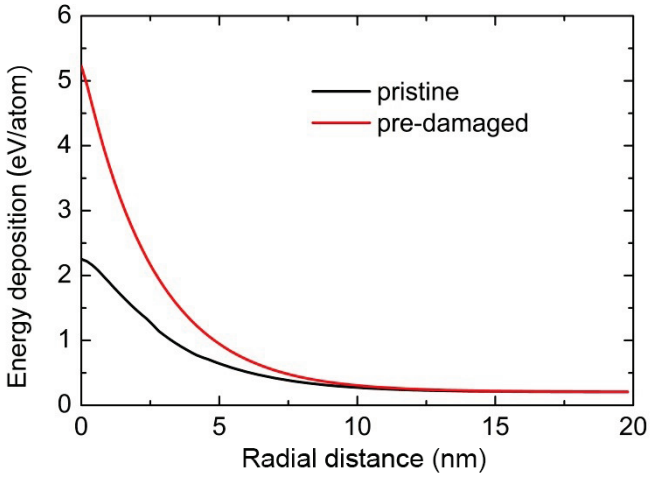

Fig. 1. Energy deposition for a 629 MeV Xe ion in pristine (black line) and pre-damaged (red line) single crystal $SrTiO_3$ as a function of radial distance from the ion trajectory.

Figure 2

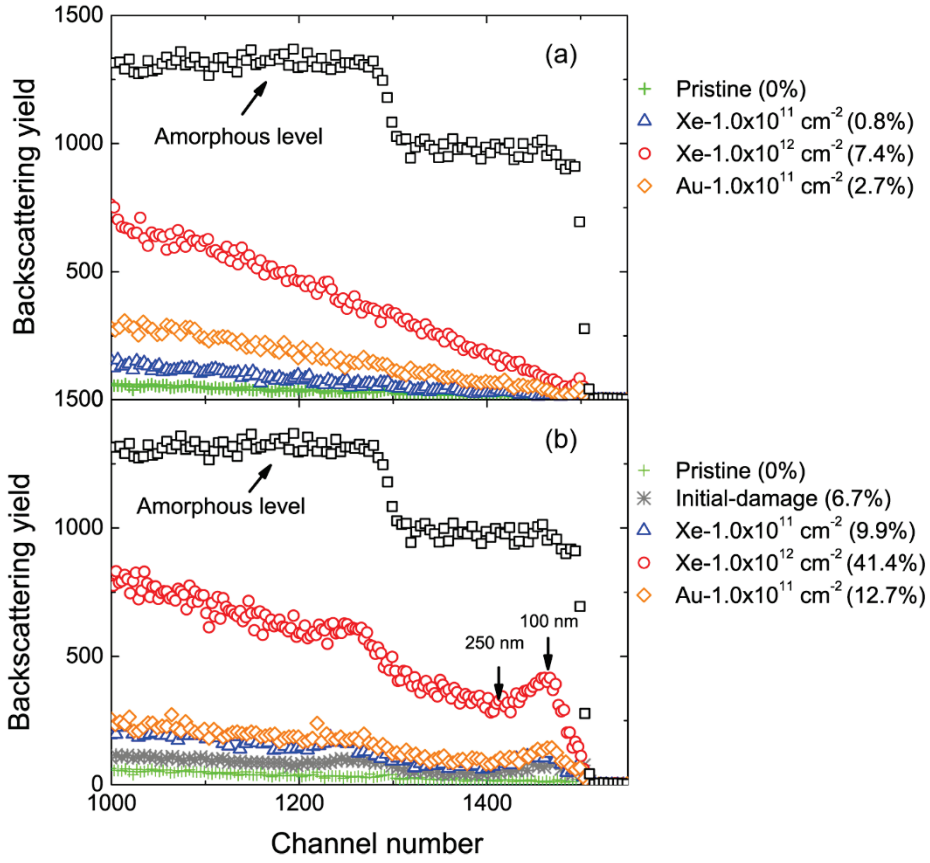

Fig. 2. Several RBS/C spectra, after irradiations with 629 MeV Xe and 946 MeV Au ions, for: (a) pristine $SrTiO_3$ without pre-damage, and (b) defective $SrTiO_3$ with a maximum disorder level of 0.06. The ratio relative to the random yield at 100 nm in depth (channel number ~1460) is labeled for each irradiation condition.

Figure 3

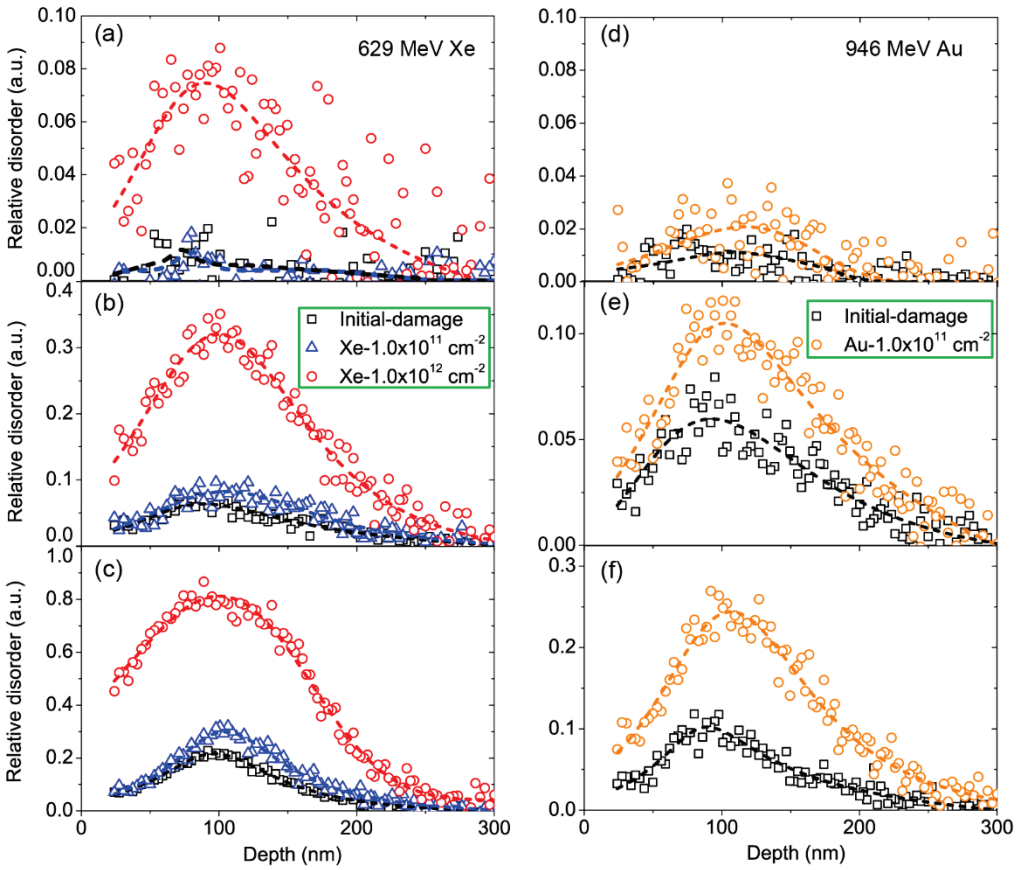

Fig. 3. The relative disorder profiles of defective $SrTiO_3$ as the function of depth before and after SHI irradiations. The 629 MeV Xe ion irradiations were performed on pre-damaged regions with maximum disorder levels of (a) ~0.01, (b) 0.06 and (c) 0.21; and the 946 MeV Au irradiations were performed on pre-damaged regions with maximum disorder levels of (d) ~0.01, (e) 0.06 and (f) 0.10. The statistical error is represented by the scattered data points from the fitted lines.

Figure 4

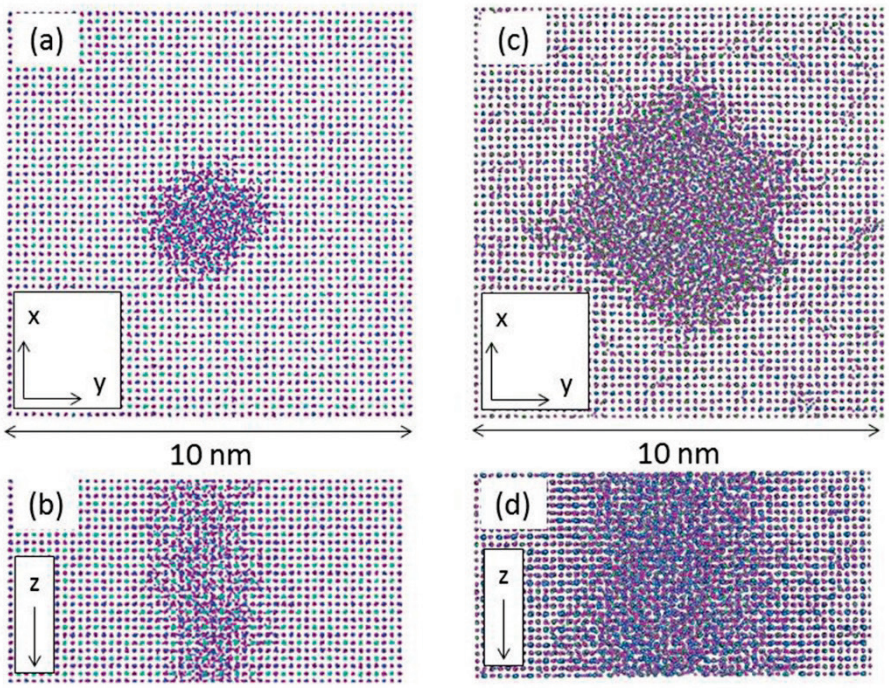

Fig. 4. (a) Cross section of the xy-plane and (b) perpendicular view along the identical ion paths of four consecutive 629 MeV Xe ions in pristine $SrTiO_3$; the consecutive ion events were at intervals of 20 ps with a total simulation time of 100 ps, and the ion trajectories were separated by 2 to 4 nm. (c) Cross section of the xy-plane and (d) perpendicular view along the path of a single Xe ion in pre-damaged $SrTiO_3$, with a total simulation time of 30 ps.

Figure 5

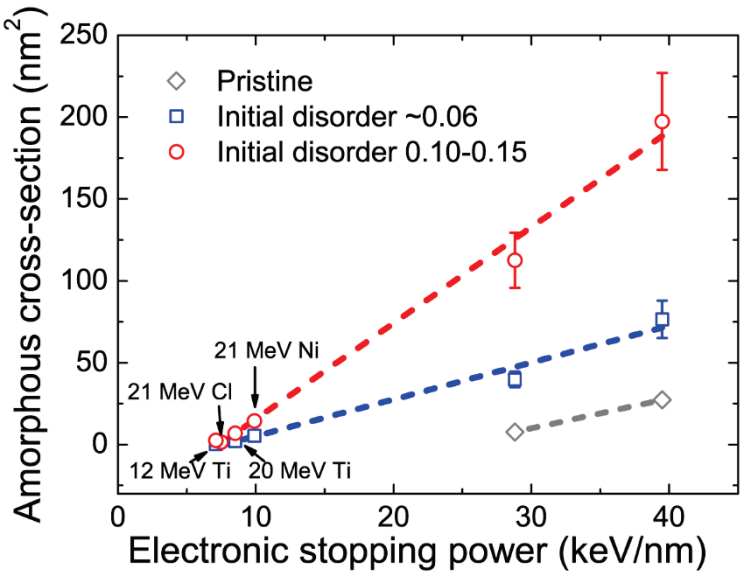

Fig. 5. Amorphous cross-sections of ion tracks as a function of dE/dx_{ele} determined at different initial disorder levels. The results for 629 MeV Xe and 946 MeV Au ion irradiations are combined with previous [33] and unpublished results for 21 MeV Ni, 21 MeV Cl, 20 MeV and 12 MeV Ti ion irradiations. Also included are the average cross sections for discontinuous tracks in pristine $SrTiO_3$. The fitting error and the experiment uncertainty (15%) have been considered and are shown by the error bars.

Figure 6

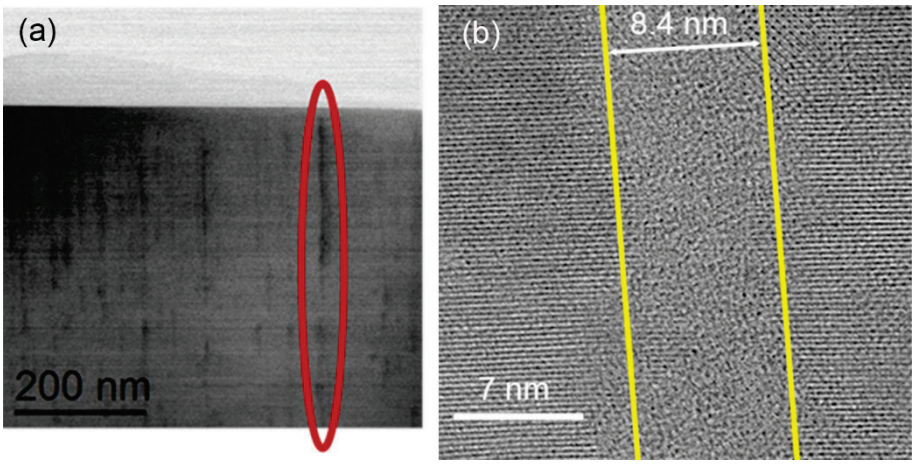

Fig. 6. ABF images of ion tracks produced in pre-damaged $SrTiO_3$ irradiated using 629 MeV Xe ions, with a disorder level of 0.10 over a depth of ~200 nm: (a) lower magnification image showing continuous tracks over the first ~200 nm of depth and discontinuous tracks at great depths in essentially pristine $SrTiO_3$; (b) high magnification image of the amorphous track in defective $SrTiO_3$ indicated in (a).

Supplementary Material

Synergistically-enhanced ion track formation in pre-damaged strontium titanate by energetic heavy ions

Haizhou Xue [a], Eva Zarkadoula [b], Ritesh Sachan [b], Yanwen Zhang [b], Christina Trautmann [c, d], and William J. Weber [a,b*]

[a] *Department of Materials Science & Engineering, University of Tennessee, Knoxville, Tennessee 37996, USA.*

[b] *Materials Science & Technology Division, Oak Ridge National Laboratory, Oak Ridge, Tennessee 37831, USA.*

[c] *GSI Helmholtzzentrum für Schwerionenforschung GmbH, Planckstrasse 1, Darmstadt 64291, Germany.*

[d] *Materialwissenschaft, Technische Universität Darmstadt, Darmstadt 64287, Germany.*

** To whom correspondence should be addressed:* wjweber@utk.edu

Irradiation with 900 keV Au ions was used to create the pre-damaged states employed in the present study. The ion flux was 4.2×10^{11} ions cm^{-2} s^{-1}, and ion fluences ranged from 4.4×10^{12} ions cm^{-2} to 4.6×10^{13} ions cm^{-2}. The atomic displacement profiles and ion ranges were predicted using the SRIM 2008 code [1] with full-cascade simulations. The density of $SrTiO_3$ was assumed to be 5.118 g cm^{-3}, and the displacement energies assumed for Sr, Ti and O atoms were 80 eV [2], 70 eV [3] and 45 eV [3], respectively. The profiles of local dose (displacements per atom) and implanted Au concentration (atomic %) with depth for the different ion fluences are shown in Figure S1. The damage produced by the 900 keV Au ions extends to a depth of about 250 nm. For the highest Au ion fluence (4.6×10^{13} cm^{-2}), the maximum Au

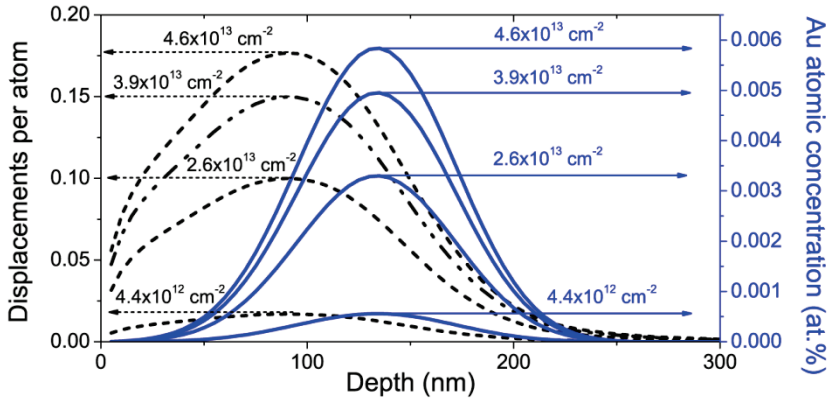

Fig. S1. SRIM-predicted local dose profile and Au atom concentration profile for 900 keV Au irradiation to different ion fluencs.

concentration is less than 0.006 at.% (<60 appm) at a depth of ~130 nm.

References

[1] J. F. Ziegler, M. D. Ziegler and J. P. Biersack (2008). *SRIM: the stopping and range of ions in matter*. Cadence Design Systems.

[2] K. L. Smith, M. Colella, R. Cooper and E. R. Vance, Measured displacement energies of oxygen ions in titanates and zirconates. Journal of nuclear materials 321 (2003) 19-28.

[3] K. L. Smith and N. J. Zaluzec, The displacement energies of cations in perovskite ($CaTiO_3$). Journal of nuclear materials 336 (2005) 261-266.